Available online at www.sciencedirect.com
SCIENCE DIRECT®
Journal of Sound and Vibration 276 (2004) 491–510
JOURNAL OF SOUND AND VIBRATION
www.elsevier.com/locate/jsvi

Aeroelastic analysis of a non-linear airfoil based on unsteady vortex lattice model

Y.H. Zhao*, H.Y. Hu

Institute of Vibration Engineering Research, Nanjing University of Aeronautics and Astronautics, 210016 Nanjing, People's Republic of China

Received 6 January 2003; accepted 4 August 2003

Abstract

Recent years have witnessed a successful model of unsteady vortex lattice to predict the limit cycle oscillations of an airfoil section. The aerodynamic model is usually in the form of discrete time, and hence, is not convenient for the analysis of non-linear aeroelastic systems. In this paper, the aerodynamic model of unsteady vortex lattice is formulated in continuous time domain and expressed in a dimensionless form. The order of aerodynamic model is greatly reduced in terms of a few aerodynamic eigenmodes to describe the unsteady vortex. Meanwhile, a static correction is included in the modal reduction to take the effects of truncated higher aerodynamic modes into account. The accuracy of the reduced-order model of aerodynamics is compared with Theodorsen's model. Using the modified aerodynamic model, the aeroelastic analysis of a two-dimensional airfoil section with combined non-linearity of freeplay and cubic stiffening in pitch is made. The numerical results indicate that the modified aerodynamic model is capable of predicting the flow about airfoil accurately and detecting the complex non-linear aeroelastic behaviors.
© 2003 Elsevier Ltd. All rights reserved.

1. Introduction

More and more airfoil models include non-linear features coming from either the structural configuration or aerodynamics. The aerodynamic non-linearities may arise from high wing angles of attack or shock waves in the transonic speed regime. The most prevalent non-linearities in structures are the cubic stiffening and the freeplay in control surface. The freeplay usually occurs in the actuated degrees of freedom, i.e., in the control surfaces with loose joints or in an advanced generic missile pin which is foldable at its settled position [1], whereas the cubic stiffening mainly comes from the large amplitude oscillation of flexible wings. Experimental data [2] of a glider

*Corresponding author. Tel.: +86-25-489-1672; fax: +86-25-489-1512.
E-mail address: hyhu@nuaa.edu.cn (Y.H. Zhao).

0022-460X/$ - see front matter © 2003 Elsevier Ltd. All rights reserved.
doi:10.1016/j.jsv.2003.08.004

showed that the combined non-linearity, of both freeplay and cubic stiffening, exists in the relation between hinge moment and pitch angle. However, few literatures deal with the aeroelastic system with this type of non-linearity. Previous studies, say [3], indicated that an airfoil section with non-linearities exhibits one of four types of motions such as the flutter, the divergence, the limit cycle oscillation and chaotic motion. The limit cycle oscillation and the chaotic motion usually occur at a flow speed much lower than the divergent flutter speed. Hence, it becomes important to know the characteristics of those non-linear oscillations in the design phase of a flight vehicle.

To authors' knowledge, Woolston and his colleagues were the first who made an attempt to study the effects of concentrated structural non-linearities by using an analog computer [4]. Recent studies on the aeroelasticity of fixed wings have focused on the identification of limit cycle oscillations in non-linear system with freeplay or cubic non-linearity. Much of this work has concentrated on the numerical or analytic algorithms to solve the non-linear aeroelastic equations, such as the point transformation method [5], the numerical continuation algorithm [6], the center manifold method [7] and the incremental harmonic balance method [8]. For the aerodynamic model used for non-linear analysis, the most prevalent one is Theodorsen's model of quasi-steady aerodynamics [8,9]. This model is based on an assumption of harmonic motion for airfoil section, and is not appropriate to predict the non-linear behavior of an aeroelastic system. Usually, the unsteady aerodynamic forces are evaluated by using Wagner's function [5,10] or Peters's finite state aerodynamic theory [11,12]. Recently, the aerodynamic model of unsteady vortex lattice, initially proposed by Hall [13], has been used to analyze the limit cycle oscillations of a cantilevered wing in low subsonic flow [14]. The model of unsteady vortex lattice does not rely on the assumption of harmonic motion for airfoil section, and describes the unsteady aerodynamic forces in time domain. Besides, it can be accurately constructed by using relatively fewer eigenmodes, and can be used to analyze non-linear aeroelastic problems.

The aeroelastic analysis of a wing relies on an accurate model of the unsteady aerodynamic forces. Because the analysis has to cope with the coupling of unsteady aerodynamic forces with structural response, the model must be in a convenient computational form. The current aerodynamic model of unsteady vortex lattice is expressed in discrete time domain so that the corresponding structural model has to be formulated in discrete time form. Such an aerodynamic model, hence, is not convenient for modelling and analysis of non-linear aeroelastic systems. In this paper, the aerodynamic model of unsteady vortex lattice is formulated in continuous time domain and expressed in a dimensionless form. A reduced-order model of aerodynamics is achieved by using modal reduction and verified by the classical Theodorsen theory of aerodynamics. For the structural non-linearities discussed above, only the combined non-linearity is considered in this paper. The non-linear aeroelastic behavior of a two-dimensional airfoil section with this type of non-linearity in pitch is investigated to illustrate the effectiveness of the modified aeroelastic model.

2. Non-linear structural equations

Fig. 1 shows a two-dimensional airfoil section of two degrees of freedom described by the plunge and the pitch. The plunge deflection h is measured at the elastic axis, positive in the

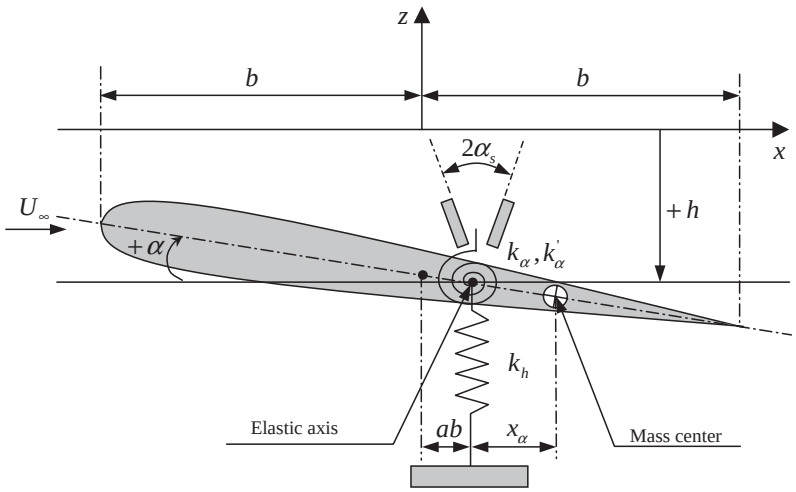

Fig. 1. Typical section of a two-dimensional airfoil with combined non-linearity.

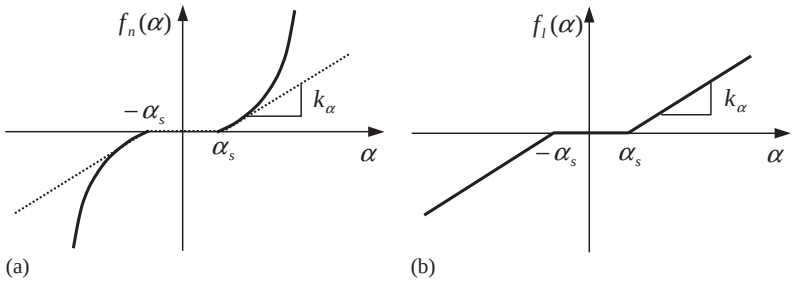

Fig. 2. Non-linear pitch stiffness: (a) combined non-linearity; (b) freeplay non-linearity.

downward direction, whereas the pitch angle α is measured from the x-axis, positive in the nose-up rotation. In addition, ab represents the distance from the elastic axis to midchord, where a is the dimensionless distance between the elastic axis and the midchord, b is the semichord of the airfoil section. The mass center of the airfoil section is located at a distance x_α from the elastic axis. k_h represents the plunge stiffness, k_α and $k_{n\alpha}$ the linear and non-linear stiffness of the cubic non-linear torsion spring, α_s the freeplay magnitude, U_∞ the flowstream velocity. The combined non-linearity and the freeplay non-linearity are shown in Fig. 2 for comparison.

The non-linear moments $f_n(\alpha)$ and $f_l(\alpha)$ can be written as

$$f_n(\alpha) = \begin{cases} k_\alpha(\alpha - \alpha_s) + k_{n\alpha}(\alpha - \alpha_s)^3, & \alpha > \alpha_s, \\ 0, & -\alpha_s \leqslant \alpha \leqslant \alpha_s, \\ k_\alpha(\alpha + \alpha_s) + k_{n\alpha}(\alpha + \alpha_s)^3, & \alpha < -\alpha_s, \end{cases} \tag{1}$$

$$f_l(\alpha) = \begin{cases} k_\alpha(\alpha - \alpha_s), & \alpha > \alpha_s, \\ 0, & -\alpha_s \leqslant \alpha \leqslant \alpha_s, \\ k_\alpha(\alpha + \alpha_s), & \alpha < -\alpha_s. \end{cases} \tag{2}$$

By using the Lagrange's equation, the equations of motion of the airfoil section with combined non-linearity can be expressed as

$$mh'' + mx_\alpha\alpha'' + k_h h = -L, \tag{3}$$

$$mx_\alpha h'' + mr_\alpha^2\alpha'' + f_a(\alpha)\alpha = M_{ea} - f_b(\alpha) - f_c(\alpha), \tag{4}$$

where the prime represents the derivative with respect to time t, m the airfoil mass per unit span, r_α the radius of gyration about elastic axis, L and M_{ea} the unsteady aerodynamic lift and moment, respectively. $f_a(\alpha)$, $f_b(\alpha)$ and $f_c(\alpha)$ are given by

$$f_a(\alpha) = \begin{cases} k_\alpha, \\ 0, \\ k_\alpha, \end{cases} \quad f_b(\alpha) = \begin{cases} -k_\alpha\alpha_s, \\ 0, \\ k_\alpha\alpha_s, \end{cases} \quad f_c(\alpha) = \begin{cases} k_{n\alpha}(\alpha - \alpha_s)^3, & \alpha > \alpha_s, \\ 0, & -\alpha_s \leqslant \alpha \leqslant \alpha_s, \\ k_{n\alpha}(\alpha + \alpha_s)^3, & \alpha < -\alpha_s. \end{cases} \tag{5}$$

To simplify the analysis, a set of dimensionless parameters is introduced as following $\omega_h^2 = k_h/m$, $\omega_\alpha^2 = k_\alpha/(mr_\alpha^2)$, $\bar{x}_\alpha = x_\alpha/b$, $\bar{r}_\alpha = r_\alpha/b$, $\bar{h} = h/b$, $\bar{\eta}_\omega = \omega_h/\omega_\alpha$, $\bar{\eta}_k = k_{n\alpha}/k_\alpha$ and $\tau = \omega_\alpha t$. Now, Eqs. (3) and (4) can be recast in a dimensionless form

$$\begin{bmatrix} 1/\bar{r}_\alpha^2 & \bar{x}_\alpha/\bar{r}_\alpha^2 \\ \bar{x}_\alpha & 1 \end{bmatrix} \begin{Bmatrix} \ddot{\bar{h}} \\ \ddot{\alpha} \end{Bmatrix} + \begin{bmatrix} \bar{\eta}_\omega^2 & 0 \\ 0 & \bar{f}_a(\alpha) \end{bmatrix} \begin{Bmatrix} \bar{h} \\ \alpha \end{Bmatrix} = \begin{Bmatrix} -Lb/k_\alpha \\ M_{ea}/k_\alpha \end{Bmatrix} - \begin{Bmatrix} 0 \\ \bar{f}_b(\alpha) \end{Bmatrix} - \begin{Bmatrix} 0 \\ \bar{f}_c(\alpha) \end{Bmatrix}, \tag{6}$$

where

$$\bar{f}_a(\alpha) = \begin{cases} 1, \\ 0, \\ 1, \end{cases} \quad \bar{f}_b(\alpha) = \begin{cases} -\alpha_s, \\ 0, \\ \alpha_s, \end{cases} \quad \bar{f}_c(\alpha) = \begin{cases} \bar{\eta}_k(\alpha - \alpha_s)^3, & \alpha > \alpha_s, \\ 0, & -\alpha_s \leqslant \alpha \leqslant \alpha_s, \\ \bar{\eta}_k(\alpha + \alpha_s)^3, & \alpha < -\alpha_s \end{cases} \tag{7}$$

and the dot represents the derivative with respect to dimensionless time τ. The non-linear aeroelastic equation (6) can be written in a compact matrix form

$$\bar{\mathbf{M}}\ddot{\mathbf{u}}(\tau) + \bar{\mathbf{K}}\mathbf{u}(\tau) = \bar{\mathbf{F}}(\tau) - \bar{\mathbf{F}}_b(\mathbf{u}(\tau)) - \bar{\mathbf{F}}_c(\mathbf{u}(\tau)), \tag{8}$$

where

$$\bar{\mathbf{M}} = \begin{bmatrix} 1/\bar{r}_\alpha^2 & \bar{x}_\alpha/\bar{r}_\alpha^2 \\ \bar{x}_\alpha & 1 \end{bmatrix}, \quad \bar{\mathbf{K}} = \begin{bmatrix} \bar{\eta}_\omega^2/\bar{r}_\alpha^2 & 0 \\ 0 & \bar{f}_a(\alpha) \end{bmatrix}, \quad \bar{\mathbf{F}}(\tau) = \begin{Bmatrix} -Lb/k_\alpha \\ M_{ea}/k_\alpha \end{Bmatrix},$$

$$\bar{\mathbf{F}}_b(\mathbf{u}(\tau)) = \begin{Bmatrix} 0 \\ \bar{f}_b(\alpha) \end{Bmatrix}, \quad \bar{\mathbf{F}}_c(\mathbf{u}(\tau)) = \begin{Bmatrix} 0 \\ \bar{f}_c(\alpha) \end{Bmatrix}, \quad \mathbf{u}(\tau) = \begin{Bmatrix} \bar{h}(\tau) \\ \alpha(\tau) \end{Bmatrix}. \tag{9}$$

3. Aerodynamic equations

3.1. Model of unsteady vortex lattice

In this section, the model of unsteady vortex lattice in a dimensionless form will be developed and formulated in continuous time domain. The flow about the airfoil section is assumed to be incompressible, inviscid and irrotational. A typical discrete model of vortex lattice for a two-dimensional airfoil section is shown in Fig. 3, where the airfoil and the wake are divided into a number of elements. The elements are all of equal size Δx in the streamwise direction. Point vortices are placed on the airfoil and the wake at the quarter chord of the elements. The airfoil section is divided into M elements representing the bound vortices, and the wake is divided into $N-M$ elements representing free vortices. The total number of vortices on both the airfoil and the wake is N. In Fig. 3, ξ_i is the location of the ith vortex, i.e., the quarter chord of each element, and $x_{i(3/4)}$ is the location of the ith collocation point, i.e., the three-quarter chord of each airfoil element. Γ_i is the strength of the ith vortex.

The dimensionless downwash induced by the discrete vortices can be expressed as

$$\bar{\mathbf{W}}_{3/4} = [\bar{\mathbf{K}}_a \ \bar{\mathbf{K}}_w] \begin{bmatrix} \bar{\mathbf{\Gamma}}_a \\ \bar{\mathbf{\Gamma}}_w \end{bmatrix}, \tag{10}$$

where the $M \times 1$ vector $\bar{\mathbf{W}}_{3/4}$ represents the dimensionless downwash at the three-quarter points of vortex elements on the airfoil section, and $\mathbf{W}_{3/4}$ represents a downwash vector such that $\bar{\mathbf{W}}_{3/4} = \mathbf{W}_{3/4}/(\omega_\alpha b)$ holds. The $M \times 1$ vector $\bar{\mathbf{\Gamma}}_a$ is the dimensionless strength of the bound vortices on the airfoil section, and $\mathbf{\Gamma}_a$ is a vector of the strength of the bound vortices yielding $\bar{\mathbf{\Gamma}}_a = \mathbf{\Gamma}_a/(\omega_\alpha b^2)$. $\bar{\mathbf{\Gamma}}_w = \mathbf{\Gamma}_w/(\omega_\alpha b^2)$, and $\mathbf{\Gamma}_w$ is the vector of the strength of the free vortices. The kernel functions in Ref. [13] can be transformed into a dimensionless form

$$[\bar{\mathbf{K}}_a]_{i,j} = \frac{1}{2\pi(\bar{x}_{i(3/4)} - \bar{\xi}_j)} \quad (1 \leqslant i \leqslant M, 1 \leqslant j \leqslant M), \tag{11}$$

$$[\bar{\mathbf{K}}_w]_{i,j} = \frac{1}{2\pi(\bar{x}_{i(3/4)} - \bar{\xi}_j)} \quad (1 \leqslant i \leqslant M, M+1 \leqslant j \leqslant N), \tag{12}$$

where $\bar{x}_{i(3/4)} = x_{i(3/4)}/b$ is the dimensionless location of the ith collocation point, and $\bar{\xi}_j = \xi_j/b$ the dimensionless location of the jth vortex. The vortex equations in the discrete time domain in

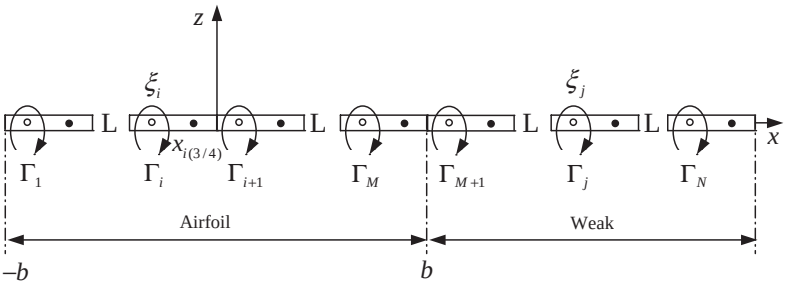

Fig. 3. Discrete model of vortex lattice for a two-dimensional airfoil section.

Refs. [13,14] can be cast in the following dimensionless form:

$$\bar{\mathbf{\Gamma}}_a^{n+1} = -\bar{\mathbf{K}}_a^{-1}\bar{\mathbf{K}}_w\bar{\mathbf{\Gamma}}_w^{n+1} + \bar{\mathbf{K}}_a^{-1}\bar{\mathbf{W}}_{3/4}^{n+1}, \tag{13a}$$

$$\bar{\mathbf{\Gamma}}_a^{n} = -\bar{\mathbf{K}}_a^{-1}\bar{\mathbf{K}}_w\bar{\mathbf{\Gamma}}_w^{n} + \bar{\mathbf{K}}_a^{-1}\bar{\mathbf{W}}_{3/4}^{n}, \tag{13b}$$

$$\bar{\Gamma}_{M+1}^{n+1} + \bar{\Gamma}_{M+1}^{n} = -2\sum_{i=1}^{M}(\bar{\Gamma}_i^{n+1} - \bar{\Gamma}_i^{n}), \tag{13c}$$

$$\bar{\Gamma}_i^{n+1} \approx \bar{\Gamma}_{i-1}^{n} \quad (i = M+2, \ldots, N-1), \tag{13d}$$

$$\bar{\Gamma}_N^{n+1} \approx \bar{\Gamma}_{N-1}^{n} + w\bar{\Gamma}_N^{n}, \quad (0.95 < w < 1), \tag{13e}$$

where the superscripts n and $n+1$ represent two moments at discrete time domain. The relaxation factor w in Eq. (13e) plays a role in preventing a sudden change in the induced downwash due to the finite length of the wake vortex sheet. From Eq. (13), the aerodynamic governing equations can be written as

$$\mathbf{A}_d\bar{\mathbf{\Gamma}}_w^{n+1} = \mathbf{B}_d\bar{\mathbf{\Gamma}}_w^{n} + \mathbf{C}_d\dot{\bar{\mathbf{W}}}_{3/4}^{n+1}, \tag{14}$$

where

$$\mathbf{A}_d = \begin{bmatrix} -2\mathbf{S} \\ \mathbf{0} \end{bmatrix}\bar{\mathbf{K}}_a^{-1}\bar{\mathbf{K}}_w + \mathbf{I}_{N-M}, \quad \mathbf{B}_d = \begin{bmatrix} -2\mathbf{S} \\ \mathbf{0} \end{bmatrix}\bar{\mathbf{K}}_a^{-1}\bar{\mathbf{K}}_w + \mathbf{C}_w, \quad \mathbf{C}_d = \begin{bmatrix} -2\mathbf{S} \\ \mathbf{0} \end{bmatrix}\bar{\mathbf{K}}_a^{-1}\Delta\tau,$$

$$\mathbf{S} = [1 \;\; 1 \;\; \cdots \;\; 1]_{1\times M}, \quad \mathbf{C}_w = \begin{bmatrix} -1 & 0 & 0 & \cdots & 0 \\ 1 & 0 & 0 & \cdots & 0 \\ 0 & 1 & 0 & \cdots & 0 \\ \cdots & \cdots & \cdots & \cdots & \cdots \\ 0 & 0 & 0 & 1 & w \end{bmatrix}_{(N-M)\times(N-M)}. \tag{15}$$

In continuous time domain, the vortex relations can be established as follows:

$$[-\mathbf{S}]\dot{\bar{\mathbf{\Gamma}}}_a = \frac{\bar{\Gamma}_{M+1}}{\Delta\bar{x}}U, \tag{16a}$$

$$\dot{\bar{\Gamma}}_i \approx -U\frac{\bar{\Gamma}_{i-1} - \bar{\Gamma}_{i+1}}{2\Delta\bar{x}} \quad (i = M+2, \ldots, N-2), \tag{16b}$$

$$\dot{\bar{\Gamma}}_{N-1} \approx -U\frac{\bar{\Gamma}_{N-2} - \bar{\Gamma}_{N-1}}{\Delta\bar{x}}, \quad \dot{\bar{\Gamma}}_N \approx -U\frac{\bar{\Gamma}_{N-1} - (w-1)\bar{\Gamma}_N}{\Delta\bar{x}}, \tag{16c}$$

where $U = U_\infty/(\omega_\alpha b)$ is the reduced velocity, $\Delta\bar{x} = \Delta x/b = U\Delta\tau$ the dimensionless size of each vortex element in the streamwise direction. It should be noted that Eq. (16a) can be derived from the conservation of vorticity. Using the finite difference equations given above, the aerodynamic governing equations can be converted into the following form in continuous time domain:

$$\mathbf{A}_c\dot{\bar{\mathbf{\Gamma}}}_w = \frac{U}{\Delta\bar{x}}\mathbf{B}_c\bar{\mathbf{\Gamma}}_w + \mathbf{C}_c\dot{\bar{\mathbf{W}}}_{3/4}, \tag{17}$$

where

$$\mathbf{A}_c = \begin{bmatrix} \mathbf{S} \\ \mathbf{0} \end{bmatrix} \bar{\mathbf{K}}_a^{-1} \bar{\mathbf{K}}_w + \begin{bmatrix} 0 & \mathbf{0} \\ \mathbf{0} & \mathbf{I}_{N-M-1} \end{bmatrix}, \quad \mathbf{C}_c = \begin{bmatrix} \mathbf{S} \\ \mathbf{0} \end{bmatrix} \bar{\mathbf{K}}_a^{-1}. \tag{18}$$

Now, attention is paid to the expression of matrix $\mathbf{B}_c$. Because the discrete model describes the behavior of trailing wake adequately, it is recommended that the discrete model be converted to a continuous one in the following manner. Note that the downwash vector $\dot{\bar{\mathbf{W}}}_{3/4}$ in Eq. (17) serves as an input to the vortex system. The homogeneous part of continuous model in Eq. (17) yields

$$\dot{\bar{\mathbf{\Gamma}}}_w = \frac{U}{\Delta \bar{x}} \mathbf{A}_c^{-1} \mathbf{B}_c \bar{\mathbf{\Gamma}}_w. \tag{19}$$

By integrating Eq. (19) from τ^n to τ^{n+1}, one can relate the discrete model to the continuous model as

$$\bar{\mathbf{\Gamma}}_w^{n+1} = \mathbf{A}_d^{-1} \mathbf{B}_d \bar{\mathbf{\Gamma}}_w^n = \exp\left\{ \left(\frac{1}{\Delta\tau} \mathbf{A}_c^{-1} \mathbf{B}_c \right) \Delta\tau \right\} \bar{\mathbf{\Gamma}}_w^n, \tag{20}$$

whereby one obtains

$$\mathbf{B}_c = \mathbf{A}_c \ln(\mathbf{A}_d^{-1} \mathbf{B}_d). \tag{21}$$

Once matrix $\mathbf{B}_c$ is determined from Eq. (21), the unsteady lift L and the moment M_{ea} can be derived from the Bernoulli's equation given by

$$L = \rho U_\infty \sum_{j=1}^{M} \Gamma_j + \rho \sum_{j=1}^{M} \sum_{k=1}^{j} \Gamma'_k \Delta x, \tag{22a}$$

$$M_{ea} = -\rho U_\infty \sum_{j=1}^{M} (\xi_j - ab) \Gamma_j - \rho \sum_{j=1}^{M} (\xi_j - ab) \sum_{k=1}^{j} \Gamma'_k \Delta x, \tag{22b}$$

where ρ is the air density and the prime represents the derivative with respect to time t.

3.2. Reduced-order model

In structural dynamics, the dynamic model of a complex structure is often reduced to a simple one of a few degrees of freedom by using modal reduction. Recently, this procedure has been applied to simplifying the models of unsteady aerodynamics [11–13]. On the basis of the reduced-order model, it may be possible to predict the unsteady aerodynamic response of a complex system over a wide frequency range. In this section, the modal reduction, which can extract the most important aerodynamic modes, is used to reduce the order of the aerodynamic equations.

Because some eigenvalues of the aerodynamic system governed by Eq. (19) may be complex, a modal reduction is used to transform the aerodynamic matrix into a canonical form first so as to make all entries in the matrix equation real. The aerodynamic system described by Eq. (19) with factor $U/\Delta\bar{x}$ being unit can be assumed to have m real eigenvalues $-\lambda_{(i)}$ $(1 \leqslant i \leqslant m)$ with corresponding right eigenvector $\psi_{\lambda(i)}$, and n pairs of complex eigenvalues $\sigma_{(k)}, \sigma^*_{(k)} = -\omega_{R(k)} \pm \mathrm{j}\omega_{I(k)}$ $(1 \leqslant k \leqslant n)$ with corresponding right eigenvector $\psi_{\sigma(k)}, \psi^*_{\sigma(k)}$. Thus, the aerodynamic matrix can be transformed into a canonical form, where a pair of complex conjugate eigenvalues

appears in a 2×2 block on the diagonal, and m real eigenvalues show up on the diagonal. Hence, the linear transform of concern can be performed as follows:

$$\mathbf{\Lambda} = \mathbf{\Phi}^{\mathrm{T}}(\mathbf{A}_c^{-1}\mathbf{B}_c)\mathbf{\Psi}, \quad \mathbf{\Phi}^{\mathrm{T}}\mathbf{\Psi} = \mathbf{I}_{N-M}, \tag{23}$$

where $\mathbf{\Phi}$ is a matrix composed of normalized left eigenvectors of the aerodynamic governing equations, and matrices $\mathbf{\Lambda}$ and $\mathbf{\Psi}$ are given by

$$\mathbf{\Lambda} = \text{Block diag}(-\lambda_{(1)}, -\lambda_{(2)}, \ldots, -\lambda_{(m)}, \mathbf{\Omega}_{(1)}, \Omega_{(2)}, \ldots, \mathbf{\Omega}_{(n)}), \quad \mathbf{\Omega}_{(i)} = \begin{bmatrix} -\omega_{R(i)} & \omega_{I(i)} \\ -\omega_{I(i)} & -\omega_{R(i)} \end{bmatrix},$$

$$\mathbf{\Psi} = [\psi_{\lambda(1)}, \psi_{\lambda(2)}, \ldots, \psi_{\lambda(m)}, \mathrm{Re}(\psi_{\sigma(1)}), \mathrm{Im}(\psi_{\sigma(1)}), \ldots, \mathrm{Re}(\psi_{\sigma(n)}), \mathrm{Im}(\psi_{\sigma(n)})]. \tag{24}$$

Now, one is in the position to establish the modal transform. To take the static effect of truncated higher modes on the system dynamics into account, a static correction is included in the modal reduction such that the modal transform is of the following form:

$$\bar{\mathbf{\Gamma}}_w = \mathbf{\Psi}_R\mathbf{q} + \bar{\mathbf{\Gamma}}_s, \tag{25}$$

where $\mathbf{\Psi}_R$ is a $(N - M) \times R$ matrix whose columns are the R columns of $\mathbf{\Psi}$ corresponding to the first R eigenvalues most close to the origin, $\mathbf{q}$ the new generalized co-ordinate vector, $\bar{\mathbf{\Gamma}}_s$ the static correction part, similar to that in the mode acceleration method for structural dynamics, so as to take the effects of truncated higher modes into account. Furthermore, the static correction can be expressed in the form

$$\bar{\mathbf{\Gamma}}_s = \bar{\mathbf{\Gamma}}_{ws} - \mathbf{\Psi}_R\mathbf{q}_s, \tag{26}$$

where $\bar{\mathbf{\Gamma}}_{ws}$ is the solution of the following equation:

$$\frac{U}{\Delta\bar{x}}\mathbf{B}_c\bar{\mathbf{\Gamma}}_{ws} + \mathbf{C}_c\dot{\bar{\mathbf{W}}}_{3/4} = 0, \tag{27}$$

whereas the quasi-static solution $\mathbf{q}_s$ can be written as

$$\mathbf{q}_s = -\frac{\Delta\bar{x}}{U}\mathbf{\Lambda}_R^{-1}\mathbf{\Phi}_R^{\mathrm{T}}\mathbf{A}_c^{-1}\mathbf{C}_c\dot{\bar{\mathbf{W}}}_{3/4}, \tag{28}$$

where $\mathbf{\Lambda}_R$ is an $R \times R$ sub-matrix whose non-zero entries are those of $\mathbf{\Lambda}$ corresponding to the R retained eigenvalues, and $\mathbf{\Phi}_R$ is a matrix whose columns are the R columns of $\mathbf{\Phi}$ corresponding to the first R eigenvalues most close to the origin. Substituting Eqs. (27) and (28) into Eq. (26), one obtains the static correction part $\bar{\mathbf{\Gamma}}_s$ as follows:

$$\bar{\mathbf{\Gamma}}_s = \frac{\Delta\bar{x}}{U}(-\mathbf{B}_c^{-1} + \mathbf{\Psi}_R\mathbf{\Lambda}_R^{-1}\mathbf{\Phi}_R^{\mathrm{T}}\mathbf{A}_c^{-1})\mathbf{C}_c\dot{\bar{\mathbf{W}}}_{3/4}. \tag{29}$$

4. Aeroelastic equations

In order to establish the aeroelastic equations, the unsteady lift L and the moment M_{ea} obtained in Section 3.1 are recast into the following form:

$$L = \rho\omega_\alpha^2 b^3\left(U\sum_{j=1}^{M}\bar{\Gamma}_j + \sum_{j=1}^{M}\sum_{k=1}^{j}\dot{\bar{\Gamma}}_k\Delta\bar{x}\right), \tag{30a}$$

$$M_{ea} = -\rho\omega_\alpha^2 b^4 \left(U \sum_{j=1}^{M} (\bar{\xi}_j - a)\dot{\bar{\Gamma}}_j + \sum_{j=1}^{M} (\bar{\xi}_j - a) \sum_{k=1}^{j} \dot{\bar{\Gamma}}_k \Delta\bar{x} \right). \tag{30b}$$

On the basis of Eqs. (8) and (30), the aeroelastic equations of motion for the two-dimensional airfoil section can be written as

$$\bar{\mathbf{M}}\ddot{\mathbf{u}}(\tau) + \bar{\mathbf{K}}\mathbf{u}(\tau) = U\bar{\mathbf{Q}}_1\bar{\mathbf{\Gamma}}_a + \bar{\mathbf{Q}}_2\dot{\bar{\mathbf{\Gamma}}}_a - \bar{\mathbf{F}}_b(\mathbf{u}) - \bar{\mathbf{F}}_c(\mathbf{u}), \tag{31}$$

where

$$\begin{aligned}
&\bar{\mathbf{Q}}_1 = \frac{1}{\pi\mu r_\alpha^2}\begin{bmatrix} -\mathbf{F}_1 \\ \mathbf{G}_1 \end{bmatrix}, \quad \bar{\mathbf{Q}}_2 = \frac{1}{\pi\mu r_\alpha^2}\begin{bmatrix} -\mathbf{F}_2 \\ \mathbf{G}_2 \end{bmatrix}, \\
&\mathbf{F}_1 = [1 \;\; 1 \;\; \cdots \;\; 1]_{1\times M}, \quad \mathbf{F}_2 = \Delta\bar{x}[M \;\; M-1 \;\; \cdots \;\; 1]_{1\times M}, \\
&\mathbf{G}_1 = -[(\bar{\xi}_1 - a) \;\; (\bar{\xi}_2 - a) \;\; \cdots \;\; (\bar{\xi}_M - a)], \quad \mathbf{G}_2 = -\Delta\bar{x}[\bar{h}_1\bar{h}_2\cdots\bar{h}_M], \\
&\bar{h}_k = \sum_{j=k}^{M} \bar{\xi}_j - (M-k+1)a \quad (1 \leqslant k \leqslant M),
\end{aligned} \tag{32}$$

and $\mu = m/(\pi\rho b^2)$ is the mass ratio.

At each collocation point of vortex element, the velocity induced by the discrete vortices should be equal to the downwash arising from the unsteady motion of the airfoil. The dimensionless downwash related to the motion of airfoil section can be written as

$$\bar{\mathbf{W}}_{3/4} = \mathbf{E}_1\dot{\mathbf{u}}(\tau) + U\mathbf{E}_2\mathbf{u}(\tau), \tag{33}$$

where

$$\begin{aligned}
&\mathbf{E}_1 = [\mathbf{S}^{\mathrm{T}} \;\; \mathbf{D}], \quad \mathbf{E}_2 = [\mathbf{0}_{M\times 1} \;\; \mathbf{S}^{\mathrm{T}}], \\
&\mathbf{D} = [(\bar{x}_{(1)3/4} - a)(\bar{x}_{(2)3/4} - a)\cdots(\bar{x}_{(M)3/4} - a)]^{\mathrm{T}}.
\end{aligned} \tag{34}$$

Combining Eqs. (10), (17), (31) with (33), eliminating $\dot{\bar{\mathbf{\Gamma}}}_a$ and applying the modal transform in Eq. (25), one arrives at the aeroelastic equation of two-dimensional airfoil section in the state space as follows:

$$\bar{\mathbf{A}}(U)\dot{\mathbf{y}}(\tau) = \bar{\mathbf{B}}(U)\mathbf{y}(\tau) - \bar{\mathbf{H}}_b(\mathbf{y}(\tau)) - \bar{\mathbf{H}}_c(\mathbf{y}(\tau)), \tag{35}$$

where

$$\begin{aligned}
&\bar{\mathbf{A}}(U) = \begin{bmatrix} \mathbf{I}_{R\times R} & U\bar{\mathbf{A}}_{c12} & \bar{\mathbf{A}}_{c13} \\ \mathbf{0}_{2\times R} & \mathbf{I}_{2\times 2} & \mathbf{0}_{2\times 2} \\ \bar{\mathbf{A}}_{c31} & U\bar{\mathbf{A}}_{c32} & \bar{\mathbf{A}}_{c33} \end{bmatrix}, \quad \bar{\mathbf{B}}(U) = \begin{bmatrix} (U/\Delta\bar{x})\mathbf{\Lambda}_R & \mathbf{0}_{R\times 2} & U\bar{\mathbf{B}}_{c13} \\ \mathbf{0}_{2\times R} & \mathbf{0}_{2\times 2} & \mathbf{I}_{2\times 2} \\ U\bar{\mathbf{B}}_{c31} & -\bar{\mathbf{K}} + U^2\bar{\mathbf{B}}_{c32} & U\bar{\mathbf{B}}_{c33} \end{bmatrix}, \\
&\bar{\mathbf{H}}_b(\mathbf{y}(\tau)) = \begin{Bmatrix} \mathbf{0}_{R\times 1} \\ \mathbf{0}_{2\times 1} \\ \bar{\mathbf{F}}_b(\mathbf{u}(\tau)) \end{Bmatrix}, \quad \bar{\mathbf{H}}_c(\mathbf{y}(\tau)) = \begin{Bmatrix} \mathbf{0}_{R\times 1} \\ \mathbf{0}_{2\times 1} \\ \bar{\mathbf{F}}_c(\mathbf{u}(\tau)) \end{Bmatrix}, \quad \mathbf{y}(\tau) = \begin{Bmatrix} \mathbf{q}(\tau) \\ \mathbf{u}(\tau) \\ \dot{\mathbf{u}}(\tau) \end{Bmatrix}.
\end{aligned} \tag{36}$$

The entries in matrix $\bar{\mathbf{A}}(U)$ and $\bar{\mathbf{B}}(U)$ are listed in Appendix A. As the dimensions of the aeroelastic equations of motion are $(R+4)$, and $\bar{\mathbf{A}}(U)$, $\bar{\mathbf{B}}(U)$ are functions of the reduced

velocity U, it is convenient to take reduced velocity U as a bifurcation parameter for non-linear analysis.

5. Comparison with Theodorsen's theory

To verify the modified aerodynamic model developed in previous sections, the classical Theodorsen's theory is used herein for comparison. For this purpose, another dimensionless time $\tau' = U_\infty t/b$ is introduced for convenience. The unsteady lift coefficient derived from Theodorsen's theory is given in Appendix B. For the reduced-order model of aerodynamics developed in previous sections, the unsteady lift coefficient can be written as

$$C_L = \mathbf{F}_1 \bar{\mathbf{\Gamma}}_Q + \mathbf{F}_2 \dot{\bar{\mathbf{\Gamma}}}_Q, \tag{37}$$

where

$$\bar{\mathbf{\Gamma}}_Q = -\bar{\mathbf{K}}_a^{-1} \bar{\mathbf{K}}_w \mathbf{\Psi}_R \mathbf{q} + \bar{\mathbf{K}}_a^{-1} \left(\mathbf{E}_1 \begin{Bmatrix} \dot{\bar{h}} \\ \dot{\alpha} \end{Bmatrix} + \mathbf{E}_2 \begin{Bmatrix} \bar{h} \\ \alpha \end{Bmatrix} \right), \tag{38a}$$

$$\dot{\mathbf{q}} = \frac{1}{\Delta \bar{x}} \mathbf{\Phi}_R^{\mathrm{T}} \mathbf{A}_c^{-1} \mathbf{B}_c \mathbf{\Psi}_R \mathbf{q} + \mathbf{\Phi}_R^{\mathrm{T}} \mathbf{A}_c^{-1} \mathbf{C}_c \left(\mathbf{E}_1 \begin{Bmatrix} \ddot{\bar{h}} \\ \ddot{\alpha} \end{Bmatrix} + \mathbf{E}_2 \begin{Bmatrix} \dot{\bar{h}} \\ \dot{\alpha} \end{Bmatrix} \right). \tag{38b}$$

Here, the static correction part is neglected for simplicity, and the dot represents the derivative with respect to the dimensionless time τ'. In Eqs. (37) and (38), if $\bar{h} = \bar{h}_0 \mathrm{e}^{\mathrm{i}k\tau'}$ and $\alpha = 0$ are assumed, C_h can be obtained. Similarly, $\alpha = \alpha_0 \mathrm{e}^{\mathrm{i}k\tau'}$ and $\bar{h} = 0$ result in the expression of C_α.

6. Numerical results

6.1. Model verification

This section presents a numerical study on the aeroelastic problem a two-dimensional airfoil section, where a set of dimensionless parameters are taken as those in Refs. [5,10]. Note that the procedures discussed in the previous sections do not depend on the choice of parameters. The mass ratio μ is 100, the dimensionless distance a between midchord and elastic axis is -0.5, the dimensionless distance $\bar{x}_\alpha$ between mass center and elastic axis is 0.25, the radius of gyration $\bar{r}_\alpha$ is 0.5, and the frequency ratio $\bar{\eta}_\omega$ is 0.2. The aeroelastic simulation is implemented by MATLAB platform.

Fig. 4 shows the discrete time eigenvalues and continuous time eigenvalues for the typical section. For this analysis, the airfoil and the wake were modelled through the use of 40 and 200 vortex elements, respectively. The length of the wake was taken to be 5 chord lengths, and the vortex relaxation factor w to be 0.996. As shown in Fig. 4(a), the magnitudes of all the discrete time eigenvalues are less than 1. These eigenvalues are mapped onto the left half plane corresponding to the continuous time domain so that the eigenvalues become two branches that emanate from the origin and go up and down on the left half plane. Moreover, the real parts of the branches asymptotically approach to a limit value. The real part of each eigenvalue is

indicative of the damping and the imaginary part is the damped frequency of each fluid eigenmode, which means that the aeroelastic system is asymptotically stable.

The classical Theodorsen's theory was used to verify the aerodynamic model. Based on the formula given in Section 5, the unsteady lift coefficients derived from the model of unsteady vortex lattice were computed for reduced frequency $k = 0.5$ and 1.0, respectively. Here, a total of 20 aerodynamic modes with the eigenvalues most closed to the origin, were used. Fig. 5 shows the

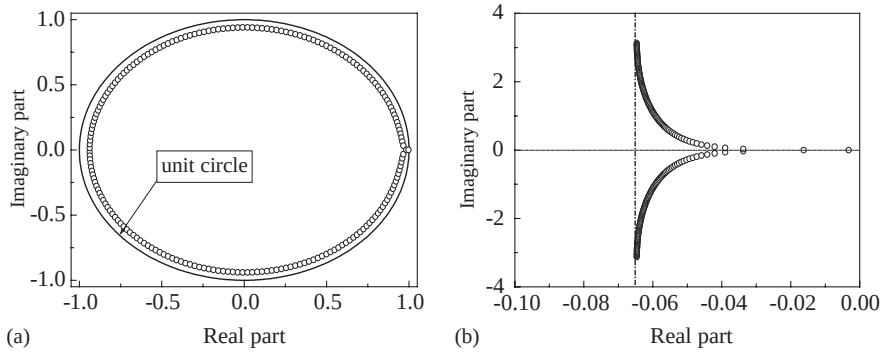

Fig. 4. Eigenvalues of an aerodynamic model: (a) discrete time; (b) continuous time.

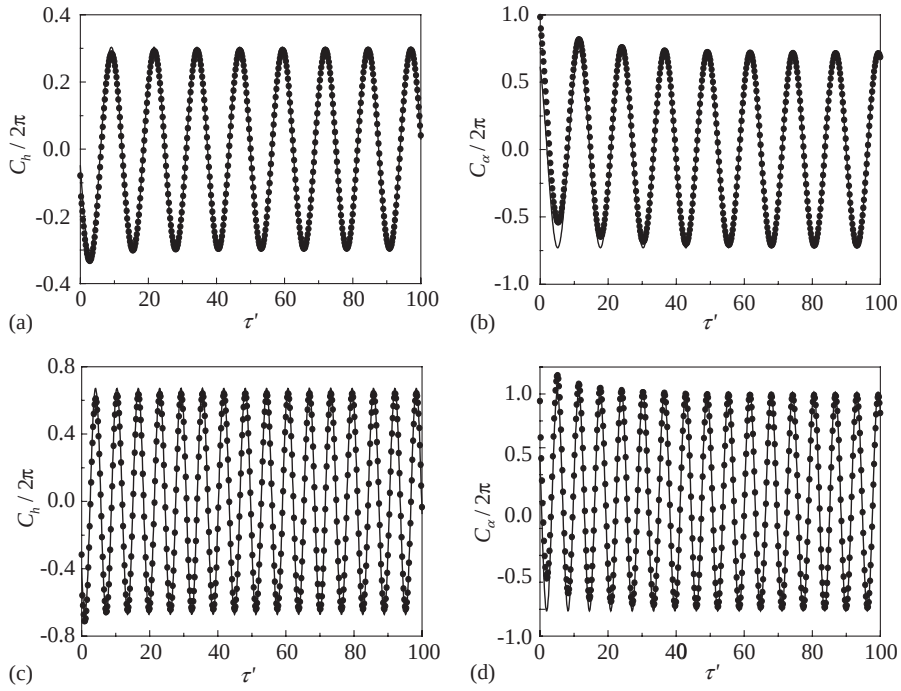

Fig. 5. Unsteady lift response: (a) $\bar{h} = \cos(k\tau')$, $k = 0.5$; (b) $\alpha = \cos(k\tau')$, $k = 0.5$; (c) $\bar{h} = \cos(k\tau')$, $k = 1.0$; (d) $\alpha = \cos(k\tau')$, $k = 1.0$; —, Theodorson's aerodynamic model; •, reduced-order model of unsteady vortex lattice with $R = 20$.

unsteady lift response of the aerodynamic system to the cosine input. Obviously, the unsteady lift response predicted by the model of vortex lattice is almost the same as that predicted by Theodorsen's aerodynamics. The comparison shows that the model of unsteady vortex lattice is able to capture the unsteady flow field quite accurately, and consequently, leads to accurate prediction of the aerodynamic forces.

In order to determine the stability of the linear aeroelastic model (i.e. $\alpha_s = 0$, $\bar{\eta}_k = 0$), the reduced-order model of aerodynamics was constructed by using a total of 20 eigenmodes. As shown in Fig. 6, the root locus method was used to predict flutter speed. For comparison, the results of the classical V–g method using Theodorsen's model were also plotted. The value g in V–g method represents the damping required for the harmonic motion, however, the frequency and g in V–g method do not have any physical meaning except at the flutter speed. The flutter speed computed by using the V–g method is $U_L \approx 6.29$, which is in good agreement with that obtained from the root locus method. These results demonstrate that the modified aerodynamic model works well.

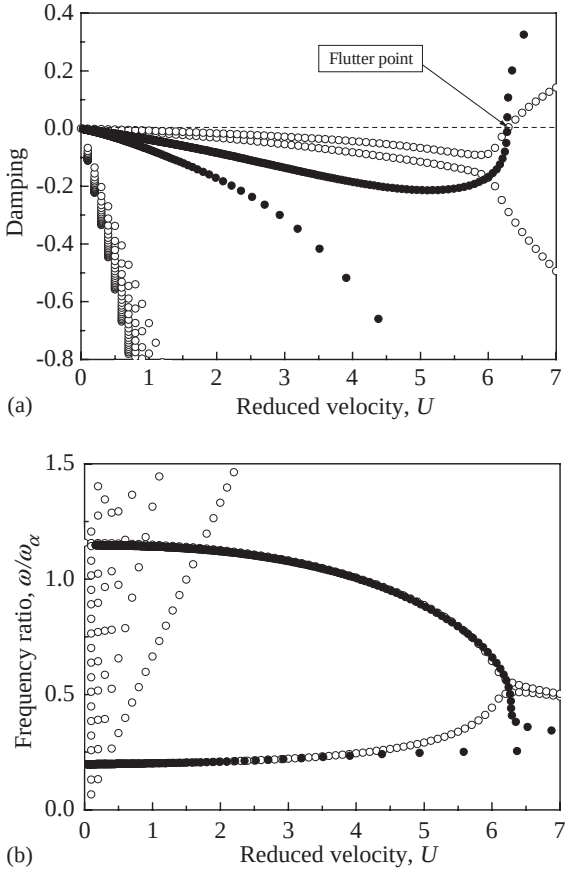

Fig. 6. Flutter analysis: (a) frequency ratio ω/ω_α versus reduced velocity U; (b) damping versus reduced velocity U. •, V–g method using Theodorson's aerodynamic model; ◦, root-locus method using reduced-order model of unsteady vortex lattice with $R = 20$.

6.2. Non-linear aeroelastic analysis

This subsection presents the analysis of non-linear aeroelastic response of the two-dimensional airfoil section which combine non-linearity by means of a standard Runge–Kutta algorithm in conjunction with the reduced-order model of aerodynamics in Eq. (35). In the computation, the freeplay magnitude α_s was taken to be 0.5°, the stiffness ratio $\bar{\eta}_k$ to be 3.0, and the number of retained aerodynamic modes to be 20. The other parameters were taken as the same as those given in Section 6.1. Now, a comparison is made in Fig. 7 by using different number of the retained aerodynamic modes. At $U/U_L = 0.3$, the limit cycle response using 20 retained aerodynamic modes is almost identical with that using 30 retained aerodynamic modes. Therefore, the higher order model of aerodynamics makes very little contribution to the system response.

A numerical simulation over a wide range of reduced velocity ratio U/U_L was performed. The initial condition used for simulation was $\alpha(0) = 3°$, and the other state variables in Eq. (35) were set to be zero. To demonstrate the complex non-linear behaviors of the system, a number of bifurcation diagrams were constructed from the response amplitude as shown in Fig. 8, where the transient responses had been damped out prior to the construction of these bifurcation diagrams. For $0 < U/U_L < 0.143$, the solution converges to an equilibrium position due to aerodynamic damping. A Hopf bifurcation can be identified at $U/U_L \approx 0.143$, with the limit cycle bifurcating from the equilibrium position via a subcritical Hopf bifurcation as shown in Fig. 9. For $U/U_L > 0.143$, the types of motion may be periodic, quasi-periodic or chaotic. As indicated in Fig. 8, there exist some amplitude jumps of plunge and pitch motions. For instance, at $U/U_L = 0.303$, 0.467, 0.550 and 0.649, the jumps of vibration amplitude appear. As illustrated in Fig. 10, the amplitude jumps are usually accompanied by the symmetric changes of phase trajectories. When $0.340 < U/U_L < 0.385$, the type of motion is quasi-periodic as shown in Fig. 11. The chaotic motions occur in three velocity regions, i.e., $0.235 < U/U_L < 0.285$, $0.385 < U/U_L < 0.450$ and $0.485 < U/U_L < 0.530$. Fig. 12 shows a chaotic motion at reduced velocity ratio $U/U_L = 0.5$.

For the aeroelastic system with freeplay non-linearity (i.e. $\alpha_s \neq 0$, $\bar{\eta}_k = 0$), flutter is divergent at any reduced velocity above the linear flutter boundary. However, for the case of combined non-linearity (i.e., $\alpha_s \neq 0$, $\bar{\eta}_k \neq 0$), as shown in Fig. 13, the flutter amplitude is bounded. The amplitude and frequency of pitch motion increase with an increase of reduced velocity ratio, and decrease

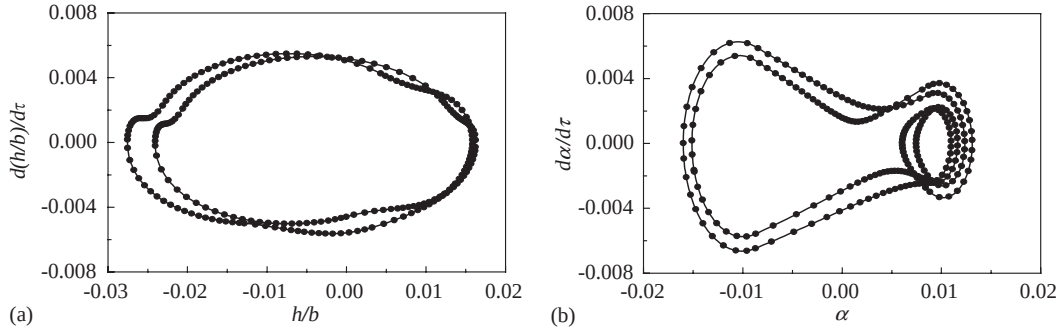

Fig. 7. Limit cycle oscillations obtained by using different number of retained aerodynamic modes, $U/U_L = 0.3$: (a) phase trajectory of plunge; (b) phase trajectory of pitch •, $R = 20$; —, $R = 30$.

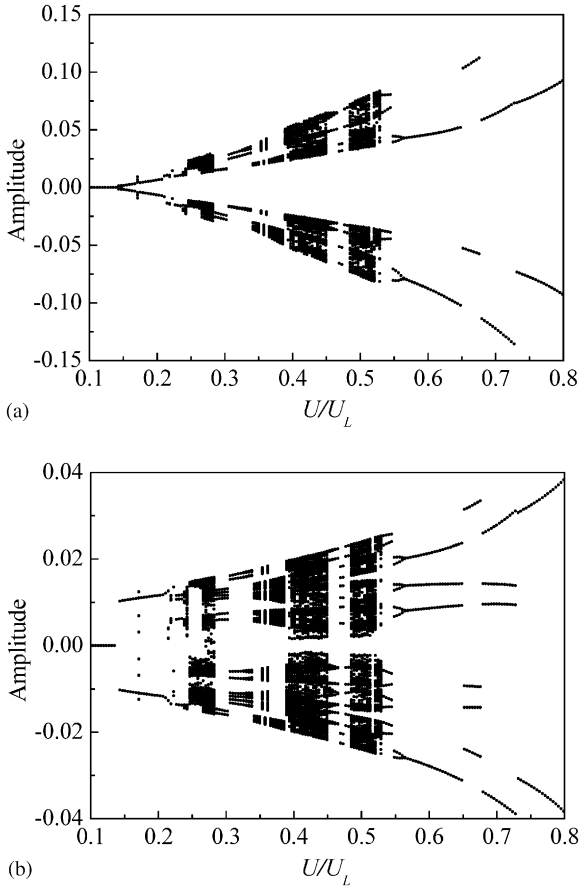

Fig. 8. Bifurcation diagrams: (a) bifurcation of plunge; (b) bifurcation of pitch.

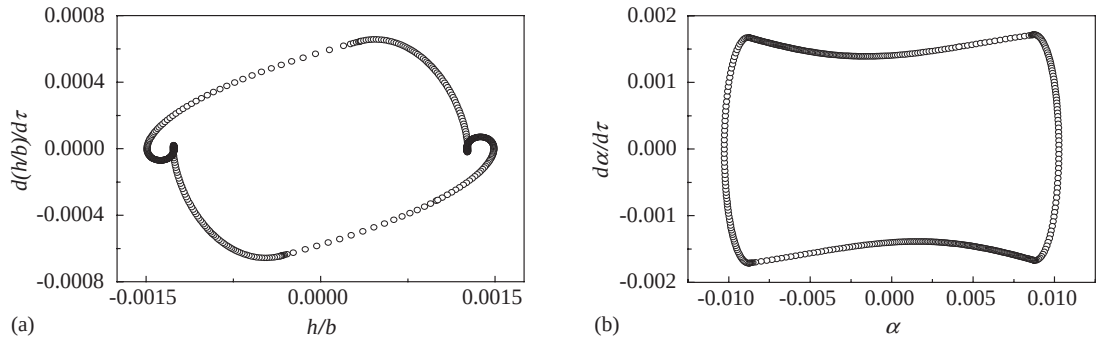

Fig. 9. Limit cycle oscillations emerged from a Hopf bifurcation, $U/U_L = 0.143$: (a) phase trajectory of plunge; (b) phase trajectory of pitch.

with an increase of stiffness ratio for a given reduced velocity ratio. From these results, it is possible to conclude that the modified aerodynamic model is effective and capable of predicting the complex non-linear behaviors of aeroelastic problems of two-dimensional airfoil sections.

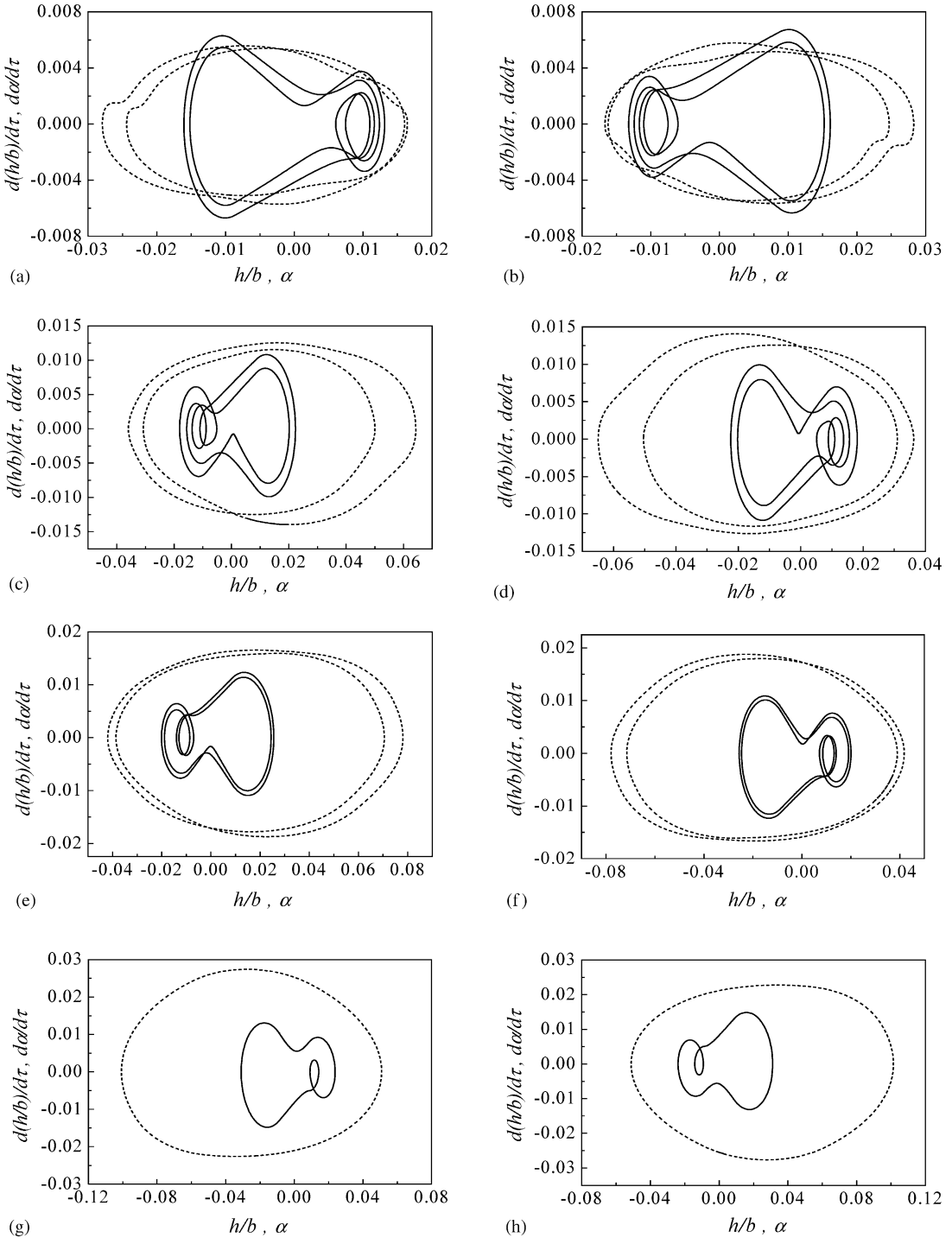

Fig. 10. Limit cycle oscillations showing symmetric trajectories: (a) $U/U_L = 0.302$; (b) $U/U_L = 0.304$; (c) $U/U_L = 0.466$; (d) $U/U_L = 0.468$; (e) $U/U_L = 0.549$; (f) $U/U_L = 0.551$; (g) $U/U_L = 0.648$; (h) $U/U_L = 0.650$. - - - -, plunge; ———, pitch.

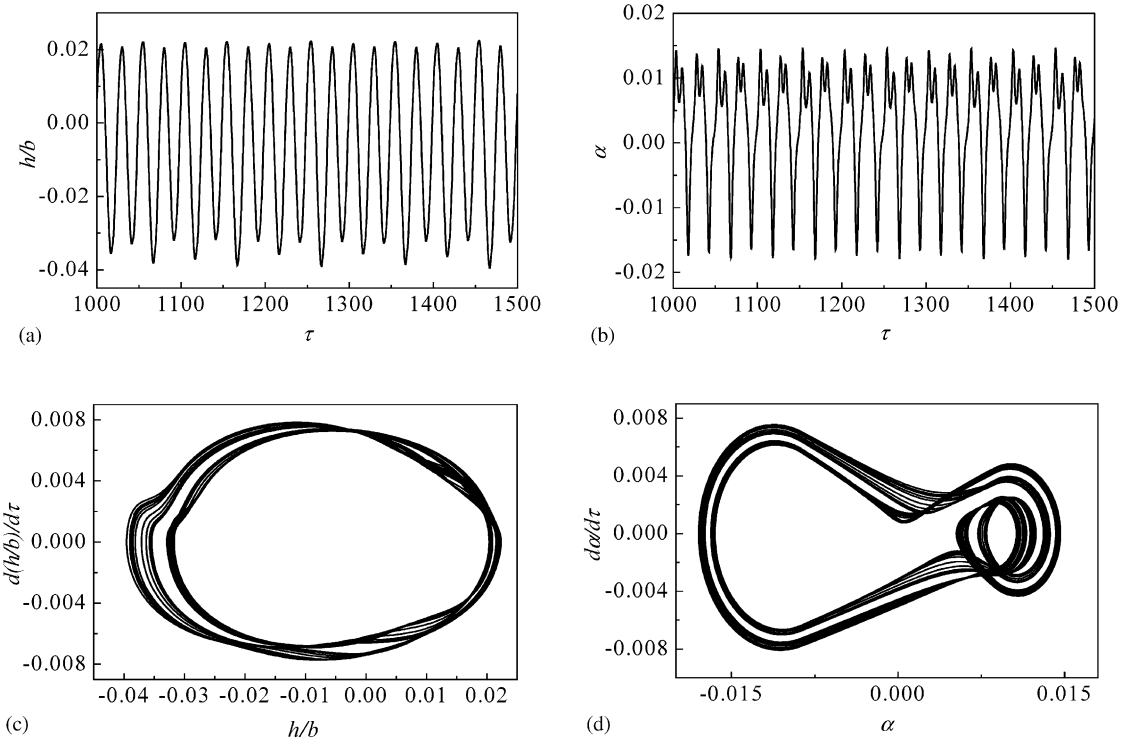

Fig. 11. Quasi-periodic motion, $U/U_L = 0.35$: (a), (b) time histories; (c), (d) phase trajectories.

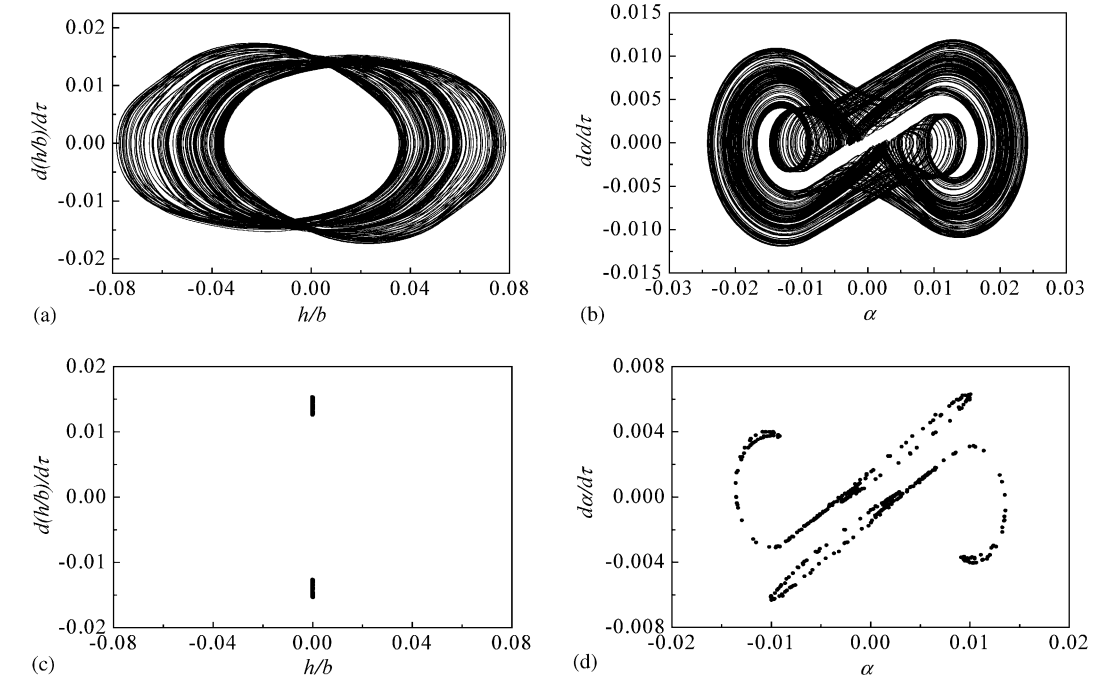

Fig. 12. Chaotic motions, $U/U_L = 0.5$: (a), (b) phase trajectories; (c), (d) strange attractors on the Poncaré section.

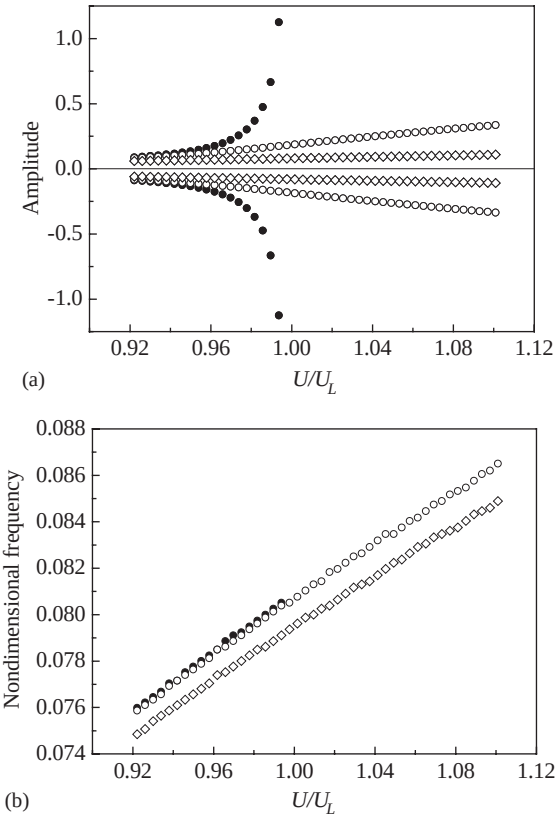

Fig. 13. The effects of stiffness ratio $\bar{\eta}_k$ on the amplitude and frequency of pitch: (a) the amplitude versus reduced velocity ratio; (b) dimensionless frequency versus reduced velocity ratio. ●, $\bar{\eta}_k = 0$; ◦, $\bar{\eta}_k = 3$; ◇, $\bar{\eta}_k = 50$.

7. Conclusions

The aerodynamic model of unsteady vortex lattice is developed in continuous time domain to describe the unsteady flow about an airfoil and the corresponding wake. The accuracy of the modified aerodynamic model is examined by using the classical Theodorsen's theory. The aeroelastic analysis is made for a two-dimensional airfoil section with combined non-linearity of freeplay and cubic stiffening on the basis of the modified aerodynamic model in conjunction with numerical integration. Periodic, quasi-periodic and chaotic motions are observed in numerical examples. The results demonstrate that the modified aerodynamic model can accurately describe the unsteady flow about the airfoil and capture the non-linear behaviors of the aeroelastic system with non-smooth non-linearity. Because the reduced-order model of aeroelasticity is established in continuous time domain, the formulas can also be conveniently used for aeroelastic control.

Acknowledgements

This work was supported in part by the National High-Tech Project under Grant 863-705-2.3.

Appendix A. Elements in matrices $\bar{\mathbf{A}}(U)$ and $\bar{\mathbf{B}}(U)$

$$\bar{\mathbf{A}}_{c12} = \mathbf{\Phi}_R^{\mathrm{T}}\mathbf{A}_c^{-1}\mathbf{A}_{c12}, \quad \bar{\mathbf{A}}_{c13} = \mathbf{\Phi}_R^{\mathrm{T}}(\mathbf{A}_c^{-1}\mathbf{A}_{c13} + \mathbf{A}_c^{-1}\mathbf{B}_c\mathbf{K}_s\mathbf{A}_{c13} - \Delta\bar{x}\mathbf{K}_s\mathbf{A}_{c12}), \tag{A.1}$$

$$\bar{\mathbf{A}}_{c31} = \mathbf{A}_{c31}\mathbf{\Psi}_R, \quad \bar{\mathbf{A}}_{c32} = \mathbf{A}_{c32}, \quad \bar{\mathbf{A}}_{c33} = \mathbf{A}_{c33} - \Delta\bar{x}(\mathbf{A}_{c31}\mathbf{K}_s\mathbf{A}_{c12} - \mathbf{B}_{c31}\mathbf{K}_s\mathbf{A}_{c13}), \tag{A.2}$$

$$\bar{\mathbf{B}}_{c13} = -\mathbf{\Phi}_R^{\mathrm{T}}\mathbf{A}_c^{-1}\mathbf{B}_c\mathbf{K}_s\mathbf{A}_{c12}, \quad \bar{\mathbf{B}}_{c31} = \mathbf{B}_{c31}\mathbf{\Psi}_R, \quad \bar{\mathbf{B}}_{c32} = \mathbf{B}_{c32},$$

$$\bar{\mathbf{B}}_{c33} = \mathbf{B}_{c33} - \Delta\bar{x}(\mathbf{B}_{c31}\mathbf{K}_s\mathbf{A}_{c12}), \tag{A.3}$$

where

$$\mathbf{K}_s = -\mathbf{B}_c^{-1} + \mathbf{\Psi}_R\mathbf{\Lambda}_R^{-1}\mathbf{\Phi}_R^{\mathrm{T}}\mathbf{A}_c^{-1}, \tag{A.4}$$

$$\mathbf{A}_{c12} = \begin{bmatrix} -\mathbf{S} \\ \mathbf{0} \end{bmatrix}\bar{\mathbf{K}}_a^{-1}\mathbf{E}_2, \quad \mathbf{A}_{c13} = \begin{bmatrix} -\mathbf{S} \\ \mathbf{0} \end{bmatrix}\bar{\mathbf{K}}_a^{-1}\mathbf{E}_1, \quad \mathbf{A}_{c31} = \bar{\mathbf{Q}}_2\bar{\mathbf{K}}_1^{-1}\bar{\mathbf{K}}_2, \tag{A.5}$$

$$\mathbf{A}_{c32} = -\bar{\mathbf{Q}}_2\bar{\mathbf{K}}_1^{-1}\mathbf{E}_2, \quad \mathbf{A}_{c33} = \bar{\mathbf{M}} - \bar{\mathbf{Q}}_2\bar{\mathbf{K}}_1^{-1}\mathbf{E}_1, \quad \mathbf{B}_{c31} = -\bar{\mathbf{Q}}_1\bar{\mathbf{K}}_1^{-1}\bar{\mathbf{K}}_2, \tag{A.6}$$

$$\mathbf{B}_{c32} = \bar{\mathbf{Q}}_1\bar{\mathbf{K}}_1^{-1}\mathbf{E}_2, \quad \mathbf{B}_{c33} = \bar{\mathbf{Q}}_1\bar{\mathbf{K}}_1^{-1}\mathbf{E}_1. \tag{A.7}$$

Appendix B. Unsteady lift coefficients based on Theodorsen's theory

In Theodorsen's theory, the harmonic plunge and pitch should be assumed, that is, $\bar{h} = \bar{h}_0 e^{ik\tau'}$ and $\alpha = \alpha_0 e^{ik\tau'}$, where $k = \omega b/U_\infty$ is the reduced frequency. Now, the unsteady lift L can be written as

$$L = \pi\rho b U_\infty^2 k^2\left[\alpha\left(\left(\tfrac{1}{2} + a\right)L_h - L_a\right) - \bar{h}L_h\right], \tag{B.1}$$

where

$$L_h = 1 - i2C(k)\frac{1}{k}, \quad L_a = \tfrac{1}{2} - i\frac{1 + 2C(k)}{k} - \frac{2C(k)}{k^2}, \tag{B.2}$$

and $C(k)$ is Theodorsen's function. The unsteady lift coefficients C_h due to the harmonic plunge input can be easily obtained

$$C_h = -\pi k^2 L_h \bar{h}_0 e^{ik\tau'}. \tag{B.3}$$

The unsteady lift coefficients C_α due to the harmonic pitch input is given by

$$C_\alpha = \pi k^2\left(\left(\tfrac{1}{2} + a\right)L_h - L_\alpha\right)\alpha_0 e^{ik\tau'}. \tag{B.4}$$

Appendix C. Nomenclature

a	dimensionless distance
b	midchord of the airfoil section
$C(k)$	Theodorsen's function
C_h	lift coefficient due to the harmonic motion of plunge
C_L	lift coefficient obtained by using the model of unsteady vortex lattice

C_α lift coefficient due to the harmonic motion of pitch
h plunge displacement at the elastic axis, positive in the downward direction
$\bar{h}$ dimensionless plunge displacement ($= h/b$)
k reduced frequency ($= \omega b/U_\infty$)
k_h translational spring stiffness
k_α, $k_{n\alpha}$ coefficients of linear and cubic stiffness of torsion spring
$\bar{\mathbf{K}}_a$, $\bar{\mathbf{K}}_w$ matrices composed of kernel functions
L unsteady aerodynamic lift
m airfoil mass per unit span
M number of elements representing the bound vortices
M_{ea} unsteady aerodynamic moment
$\bar{\mathbf{M}}$, $\bar{\mathbf{K}}$ matrices of mass and stiffness
N total number of vortices on both the airfoil and the wake
$\mathbf{q}$ generalized co-ordinate vector used in modal transform
r_α radius of gyration about elastic axis
$\bar{r}_\alpha$ dimensionless radius of gyration about elastic axis ($= r_\alpha/b$)
R number of the retained aerodynamic modes
t time
U reduced velocity ($= U_\infty/(\omega_\alpha b)$)
U_L linear flutter speed
U_∞ freestream velocity
w relaxation factor ($0.95 \leqslant w \leqslant 1$)
$\mathbf{W}_{3/4}$ downwash vector
$\bar{\mathbf{W}}_{3/4}$ dimensionless downwash vector ($= \mathbf{W}_{3/4}/(\omega_\alpha b)$)
$x_{i(3/4)}$ location of the ith collocation point
Δx size of the vortex elements in the streamwise direction ($= 2b/M$)
x_α distance between the mass center of airfoil and the elastic axis
$\bar{x}_{i(3/4)}$ dimensionless location of the ith collocation point ($= x_{i(3/4)}/b$)
$\bar{x}_\alpha$ dimensionless distance between the mass center of airfoil and the elastic axis ($= x_\alpha/b$)
α pitch angle, positive in the nose-up rotation
α_s freeplay magnitude
ρ air density
μ mass ratio ($= m/(\pi\rho b^2)$)
ξ_i location of the ith vortex
$\bar{\xi}_j$ dimensionless location of the jth vortex ($= \xi_j/b$)
ω_h uncoupled plunge natural frequency ($= (k_h/m)^{1/2}$)
ω_α uncoupled pitch natural frequency ($= (k_\alpha/(mr_\alpha^2))^{1/2}$)
$\bar{\eta}_k$ stiffness ratio ($= k_{n\alpha}/k_\alpha$)
$\bar{\eta}_\omega$ frequency ratio ($= \omega_h/\omega_\alpha$)
τ dimensionless time used for non-linear analysis ($= \omega_\alpha t$)
τ' dimensionless time used for model verification ($= U_\infty t/b$)
Γ_i strength of the ith vortex
$\mathbf{\Gamma}_a, \mathbf{\Gamma}_w$ vectors representing the strength of the bound vortices on the airfoil and free vortices on the wake, respectively

$\bar{\mathbf{\Gamma}}_a$ vector representing the dimensionless strength of the bound vortices ($= \mathbf{\Gamma}_a/(\omega_\alpha b^2)$)
$\bar{\mathbf{\Gamma}}_w$ vector representing the dimensionless strength of the free vortices ($= \mathbf{\Gamma}_w/(\omega_\alpha b^2)$)
$\bar{\mathbf{\Gamma}}_s$ static correction part in modal transform
$\mathbf{\Phi}$, $\mathbf{\Psi}$ left modal matrix, right modal matrix
$\mathbf{\Phi}_R$, $\mathbf{\Psi}_R$ modal matrices composed of R retained modes
$\mathbf{\Lambda}$ eigenvalue matrix
$\mathbf{\Lambda}_R$ $R \times R$ sub-matrix of $\mathbf{\Lambda}$ corresponding to the R retained eigenvalues

Superscripts
"$'$" derivative with respect to the dimensionless time τ or τ'
"$\cdot$" derivative with respect to time t

References

[1] D.H. Hyun, I. Lee, Transonic and low-supersonic aeroelastic analysis of a two-degree-of-freedom airfoil with a freeplay non-linearity, *Journal of Sound and Vibration* 234 (2000) 859–880.
[2] B.H.K. Lee, S.J. Price, Y.S. Wong, Nonlinear aeroelastic analysis of airfoils: bifurcation and chaos, *Progress in Aerospace Sciences* 35 (1999) 205–334.
[3] I. Lee, S.H. Kim, Aeroelastic analysis of a flexible control surface with structural nonlinearity, *Journal of Aircraft* 32 (1995) 868–874.
[4] D.S. Woolston, H.L. Runyan, R.E. Andrews, An investigation of effects of certain types of structural nonlinearities on wing and control surface flutter, *Journal of Aeronautical Sciences* 24 (1957) 57–63.
[5] L. Liu, Y.S. Wong, Nonlinear aeroelastic analysis using the point transformation method, Part I: freeplay models, *Journal of Sound and Vibration* 253 (2002) 447–469.
[6] I. Roberts, D.P. Jones, et al., Analysis of piecewise linear aeroelastic systems using numerical continuation, *Journal of Aeronautical Engineering* 216 (2002) 1–11.
[7] L. Liu, Y.S. Wong, B.H.K. Lee, Application of the center manifold theory in nonlinear aeroelasticity, *Journal of Sound and Vibration* 234 (2000) 641–659.
[8] A. Raghothama, S. Narayanan, Non-linear dynamics of a two-dimensional airfoil by incremental harmonic balance method, *Journal of Sound and Vibration* 226 (1999) 493–517.
[9] Z.C. Yang, L.C. Zhao, Chaotic motions of an airfoil with nonlinear stiffness in incompressible flow, *Journal of Sound and Vibration* 138 (1990) 245–254.
[10] S.J. Price, H. Alighanbari, B.H.K. Lee, The aeroelastic response of a two-dimensional airfoil with bilinear and cubic structural nonlinearities, *Journal of Fluids and Structures* 9 (1995) 175–193.
[11] D.M. Tang, M.D. Conner, E.H. Dowell, Reduced-order aerodynamic model and its application to a nonlinear aeroelastic system, *Journal of Aircraft* 35 (1998) 332–338.
[12] D.M. Tang, D. Kholodar, E.H. Dowell, Nonlinear response of airfoil section with control surface freeplay to gust loads, *American Institute of Aeronautics and Astronautics Journal* 38 (2000) 1543–1557.
[13] K.C. Hall, Eigenanalysis of unsteady flows about airfoils, cascades, and wings, *American Institute of Aeronautics and Astronautics Journal* 32 (1994) 2426–2432.
[14] D.M. Tang, E.H. Dowell, K.C. Hall, Limit cycle oscillations of a cantilevered wing in low subsonic flow, *American Institute of Aeronautics and Astronautics Journal* 37 (1999) 364–371.